LEWIS GRANT
IN-25-CR
99098
27P.

FINAL REPORT

NASA GRANT NAG3-368

1 October 1982 - 30 September 1986

The Temperature Dependence of Inelastic Light Scattering from Small Particles for Use in Combustion Diagnostic Instrumentation

prepared by

Stanley D. Cloud
Associate Professor of Physics
University of Nevada, Las Vegas
Las Vegas, Nevada 89154

submitted to

The National Aeronautics & Space Administration
Lewis Research Center
Cleveland, Ohio

October 9, 1987

(NASA-CR-180399) THE TEMPERATURE DEPENDENCE OF INELASTIC LIGHT SCATTERING FROM SMALL PARTICLES FOR USE IN COMBUSTION DIAGNOSTIC INSTRUMENTATION Final Report, 1 Oct. 1982 - 30 Sep. 1986 (Nevada Univ.) 27 p Avail: G3/25

N87-28634

Unclas
0099098

I. INTRODUCTION

The work described in this report falls into two parts: (1) a computer calculation of the expected angular distribution of coherent anti-Stokes Raman scattering (CARS) from micrometer size polystyrene spheres based on a Mie-type model, and (2) a pilot experiment to test the feasibility of measuring CARS angular distributions from micrometer size polystyrene spheres by simply suspending them in water. The computer calculations predict very interesting structure in the angular distributions that depends strongly on the size and relative refractive index of the spheres. The expected sharp structure makes an experiment particularly important not only as a test of the theoretical model's details but also as preliminary to a variety of possible applications.

This work grew out of a project to find means for increasing the sensitivity or applicability of CARS as a tool for combustion diagnostic instrumentation. A great deal of work has been done in the application of CARS to combustion studies[1,2], yet many problems remain to be solved. The theoretical work of Cooney and Gross[3] in 1982 showed that CARS from small particles might be enhanced by an order of magnitude over the intensity of scattering from the bulk material and by an even greater amount over the intensity of scattering from gas molecules. This suggested the possibility of seeding a flame with particles of suitable material and using CARS from the particles as a probe of local gas density and local pressure.

Since only Cooney's and Gross's computation of CARS from benzene droplets had been made and since no experiments had been performed at all, it was essential to develop a basis of scientific information about particle CARS before passing judgment on the technique as a combustion diagnostics instrumentation tool. The first step was to extend the computational capability to include any material and to produce complete angular information about CARS from a particle of any size within the limits of the Mie-type calculation. The second step was to select a convenient particle material and attempt to measure the CARS angular distribution for comparison with the calculational model.

II. THEORETICAL CALCULATIONS

The first reported computer calculations of CARS from micrometer size particles were by Cooney and Gross[3]. Due to limitations of computer facilities, they only considered CARS from benzene liquid droplets, and they only did computations for thirteen different droplet sizes. Earlier experiments[4] with fluorescence from dye-doped latex spheres had shown sharp "size resonances" that might appear in CARS also. In order to indicate the presence of such resonances, which are less than one percent in width, calculations needed to be made for a range of closely spaced particle sizes. The Cray-1S supercomputer at the Lewis Research Center made such detailed calculations possible.

Details of the Mie-type model used for the computation of CARS angular distributions from particles are contained in the Ph.D. dissertation of Gross.[5] The essential ideas are the following. In CARS, three incident photons interact simultaneously with a molecule to produce a fourth photon with a different energy. Typically, two of the incident photons are frequency-doubled Nd:YAG laser photons with a wavelength of 532nm, while the third incident photon comes from a tunable dye laser driven also by the Nd:YAG laser. The dye laser wavelength is chosen in accordance with the Raman resonance one desires to use in a particular material. If the energy of the Nd:YAG laser photons is E_1 and the energy of the dye laser photon is E_2, then the fourth photon resulting from CARS will have energy $2E_1-E_2$.

From the point of view of electric fields, in the CARS process described above, two of the incident photons induce fields in the particle that oscillate at frequency f_1 while the third induces a field oscillating at frequency f_2. The presence of these fields simultaneously superimposed in the material produces a new electromagnetic oscillation at a frequency f_3 equal to $2f_1-f_2$. The new frequency results because the material has a third-order, nonlinear susceptibility.

In order to predict the intensity and directional distribution of the new CARS produced light theoretically, the oscillation at frequency $f_3=2f_2-f_1$ is introduced as a source into Maxwell's equations. Maxwell's equations combine to form a wave equation with a source term at frequency f_3 whose intensity is a function of position within the particle. The wave equation can be solved numerically by the Green function technique and multipole expansion, subject to boundary conditions at the surface of the sphere. A mathematical outline of the procedure is given in appendix A.

The computation routine involves several steps. First, the field distributions at frequencies f_1 and f_2 are found inside the sphere in terms of the amplitudes and polarizations of the incident photon beams. To do this, the fields are expressed in terms of Ricatti-Bessel functions and associated Legendre functions. Then the distribution of sources at f_3 is calculated and integrated with the vector multipoles over the volume of the particle. The vector multipoles are computed from spherical Bessel functions and irreducible tensors, which are expressed in terms of spherical harmonics by means of the Clebsch-Gordan coefficients. Next, the integrals over the volume are combined with the boundary conditions at the surface of the sphere to yield coefficients in a multipole expansion of the scattered field. The scattered field is computed angle by angle as the partial sum of the expansion, including enough terms to give sufficient precision in the final result.

The program is exhibited in appendix B. It is very simple to use, because very little input data are required. The size parameter of the particle is input at line 3300, and the number of terms to be included in the multipole expansion at line 3400. The three wavelengths and the corresponding refractive indices are entered directly into the common block as REFRAC(3) and WAVE1(3). The entered wavelengths are those outside the particle. The program computes the wavenumbers inside the particle at line 4000.

In operation, the program begins calculating the incident fields inside the particle using subroutines MIECO and INFLD. MIECO is called at line 4200. The special functions are called, and then at line 6400, the integration of the new field over the particle volume is begun. DPROD (line 8700) is the new field at f_3. The resulting integrals are CLE and CLM, and they are the coefficients to be used in the multipole sums begun in line 14200. Output of the program is an angular distribution of the logarithm of the CARS intensity in relative units, printed at line 18600. FIT is the scattering angle in degrees measured from the direction of the incident beams. DCS is the log intensity.

The subroutines used are:

MIECO	calculates the Mie-type coefficients for use in finding the internal fields in INFLD
RBES	computes the Ricatti-Bessel functions;
RHANK	computes the Ricatti-Hankel functions;
INFLD	finds the internal fields;
LEG	calculates the Legendre functions;
YLM	computes the spherical harmonics;
TLM	computes the irreducible tensors or vector spherical harmonics;
CLG	calculates the Clebsch-Gordan coefficients.

Note that wherever possible the program is vectorized to run with optimal speed on a Cray-1 computer. For LMAX = 20, which is sufficient for size parameters up to about 8, the program runs in approximately 40 sec of CPU time. Run time increases rapidly with increasing LMAX. With LMAX = 95, the program took about 3.3 hours.

CARS angular distributions were computed on the NASA Lewis Research Center Cray-1S computer, transmitted via Telenet to an IBM-PC, and stored on floppy disks. The angular distributions were then sent by telephone line from the IBM-PC to the University of Nevada, Las Vegas Computing Center Cyber-172 computer where they were archived and plotted using the National Center for Atmospheric Research graphics package called NCAR.

The first calculations were a set of angular distributions for 29 different size parameters ranging from 5.39 to 6.79 for a polystyrene sphere immersed in air. These results are presented in figures 1, 2, and 3. The vertical scale is the logarithm of the scattered intensity on a relative scale.

Polystyrene was chosen as the material in anticipation of an experiment. Polystyrene is a polymer of styrene, whose structure includes a benzene ring. So polystyrene has Raman scattering properties very similar to benzene; in particular, it exhibits a strong, isolated Raman resonance near 1000 cm^{-1}.[6] Polystyrene spheres carefully manufactured in a range of sizes are available commercially as "uniform latex".

Figures 1 through 3 show angular distributions with considerable structure that changes rapidly at certain scattering angles as the particle size changes. The change of structure with size is a property that may be exploitable for applications. This will be discussed further in the section entitled "Discussion". However, the figures show that the change of angular distribution with size is very complicated, so great detail will be required for applications.

Figure 4 shows the variation of CARS angular distributions as the refractive index changes. The refractive index is, of course, the relative refractive index, so a change can be the result of something happening within the particle or in the surrounding medium. The figure shows that CARS scattering changes relatively slowly with refractive index. Figure 5 shows that there is practically no change in CARS angular distribution when the ambient air pressure is increased from zero to 90 atmospheres.

For the purpose of doing an experiment to compare actual CARS with the computed angular distributions, one wants a scatterer that will produce structured distributions that are not sensitive to experimental conditions. For example, in a sample of polystyrene latex there might be a variation of 1% or 2% in the sizes of the particles. If the scattering is sensitive to such small changes, then the particle distribution will smear the angular distributions. Providing the size distribution is known, it is possible to integrate over the range of angular distributions to obtain a smeared theoretical distribution. However, one should expect violently changing conditions in the vicinity of the high-powered laser beam required for CARS, and both the nature and the magnitude of the changes may be difficult to determine precisely. For example, due to heating or ablation, the actual size of the particles might change appreciably. Furthermore, the surrounding medium could expand or even vaporize if it is a liquid. In general, when the relative refractive index is reduced, the amount of structure and the size-variation of the structure in CARS angular distributions is reduced. This is seen in figures 6 and 7, which present CARS in water for a range of size parameters and for a range of refractive indices. It suggests that for a preliminary experiment, it would be desirable to suspend the particles in a medium, such as water, whose refractive index is different from that of polystyrene (approximately 1.6), so that some structure will be present. But the surrounding refractive index should not be too different. A relative refractive index of about 1.2, as shown in the figures, should give good results.

These computations were presented in a conference paper.[7]

III. EXPERIMENT

Preliminary experiments to observe CARS from polystyrene latex spheres were carried out using the Nd:YAG/Dye laser CARS system at the NASA Lewis Research Center. The plan included generating CARS from latex suspended in water held in a cell within a Wyatt Technology "Dawn Model B" fifteen-detector light scattering system.[8] The fifteen detectors were intended to detect the scattered light at fifteen angles simultaneously. Output from the detectors would be digitized and stored in a personal computer for later analysis. Interference filters[9] to transmit the CARS generated light but block directly scattered incident light were fitted in front of the fifteen detectors. Although the experiment did not proceed to the point of producing CARS within the "Dawn" system, the "Dawn" system was interfaced to the computer and tested satisfactorily as a detector system. Furthermore, the interference filters were found to discriminate very well against light from the laser beams, transmitted the CARS wavelengths as expected, and were extensively used in the pilot CARS study to be described.

Before attempting to observe CARS from polystyrene particles, an effort was made to see CARS from bulk liquid benzene. A quartz cylindrical cell filled with benzene was positioned with its flat end faces perpendicular to the approximately colinear incident beams. With the dye laser wavelength set at about 562nm and its intensity roughly one-half the intensity of the Nd:YAG laser beam at 532nm, a spot of blue light could be seen slightly off axis when the light exiting the cell was allowed to fall on a white card. It was necessary to view the card through the interference filters mentioned above in order to suppress the incident laser beams and also the yellow and red Raman shifted laser beams. The blue light was directed into a spectrometer via a prism, and the wavelength was measured to be about 505nm in agreement with the $f_3=2f_2-f_1$ expectation.

To explore the possibility of detecting CARS from polystyrene microspheres, a very dilute suspension of 1.091 micrometer latex particles[10] in water was prepared. The concentration of polystyrene in the cell was about 5×10^{-7}, which would give approximately 5 microspheres in the interaction region where the incident laser beams were focused. The dimensions of the interaction region were estimated to be 1mm of length by 0.1mm diameter. Using the interference filters to block scattered incident laser light, it was possible to observe visually blue light emerging from the region of beam focus. A fiber bundle was used to collect the blue light and direct it through a lens that focused it on the slit of a double spectrometer. To confirm that it was CARS from the polystyrene spheres, the light passing through the spectrometer was analyzed by an optical multichannel analyzer system gated synchronously with laser pulses. As expected, a wavelength peak was found at about 505nm. However, the 505nm light remained present as the dye laser wavelength was scanned over a 10nm or more range, whereas a peak with a width of perhaps $20cm^{-1}$ (see ref. 6) or about 0.6nm was expected. This "continuous" background was attributed to weak CARS from a distant Raman resonance in water. To detect the presence of polystyrene, then, it was necessary to search for a weak, narrow peak superimposed on the water background in a plot of 505nm light intensity versus dye laser wavelength.

Data collection was quite difficult because it was necessary to keep the laser beam intensities down so as to minimize damage to the cell window and also prevent boiling of the water. This meant that the signal was weak and difficult to collect efficiently with the optical fiber bundle. Integration periods of several minutes were required, during which the laser output power could drift, so laser power was monitored and regulated manually. Furthermore, whenever window damage was detected by the presence of photoacoustic pulses, the cell had to be moved slightly and the fiber bundle had to be repositioned. Average laser power was typically 13mW at 532nm and 6mw at 562nm with a 10 hertz repetition rate.

Late on the next to last day of scheduled time, just such a narrow peak was found in the day's last run. The data are shown in figure 8. Both peak position and width are as expected. Unfortunately, due to the difficulties mentioned above, it was not possible to confirm the presence of the peak.

DISCUSSION

The theoretical results indicate that CARS from particles is rich in structure. Whether the structure can be exploited efficiently for instrumentation purposes remains to be determined, and much more developmental work is needed. In particular, the fundamental question of the applicability of the Mie-type model to droplets of benzene or to polystyrene spheres has not yet been answered experimentally. The particle's surface is included in the model as an interface at which boundary conditions must match. The matching of boundary conditions requires the addition of a field in addition to that directly attributable to the sources at f_3, and that field results from the surface. But the model does not take into account that the CARS interaction might be different at the surface or that surface currents might be produced. Especially with such small particles with large surface to volume ratios under the influence of very intense incident fields, surface effects may be significant. The Yale group has been successful in observing nonlinear scattering from droplets recently[11], but they are working with larger droplets, of about 30 micrometers, rather than the approximately 1 micrometer particles considered here.

Some modifications in the apparatus should be made before further experiments are attempted. If possible, laser power stability should be improved. In any case, the scattered light collection system should be made more efficient. Perhaps CARS signal strength can be increased by using a dense aerosol of particles instead of a dilute suspension.

Although the experiment described here was conceived more optimistically than it turned out, it was nevertheless intended only as a pilot study to determine the feasibility of detecting CARS from small particles and to discover what the main barriers to success are likely to be. It was successful in those respects: CARS was observed, if only briefly from polystyrene particles; and a clear idea of the difficulties has emerged.

ACKNOWLEDGMENTS

I owe special thanks to Dr. Nancy Piltch, who very generously interrupted her own research to make her CARS facility available to me for a month, who patiently instructed me in its use, and who assisted with the experiments. Mr. Ken Weiland provided excellent and absolutely essential technical support. Dr. Arthur Decker first interested me in this project and, with Mr. Daniel Lesco, Mr. William Nieberding, and Mr. Norman Wenger, provided encouragement and support.

V. REFERENCES

1. Eesley, G. L., Coherent Raman Spectroscopy (Pergamon Press, 1981).

2. Hall, Robert J., and Alan C. Eckbreth, "Coherent Anti-Stokes Raman Spectroscopy (CARS): Application to Combustion Diagnostics," in Laser Applications Volume 5, ed. by John F. Ready and Robert K. Erf (Academic Press, Inc. 1984).

3. Cooney, John and Abraham Gross, "Coherent anti-Stokes Raman scattering by droplets in the Mie size range," Optics Letters 7, 218 (1982).

4. Benner, R. E., P. W. Barber, J. F. Owen, and R. K. Chang, "Observations of Structure Resonances in the Fluorescence Spectra from Microspheres," Physical Review Letters 44,

475 (1980).

5. Gross, Abraham, Coherent Anti-Stokes Raman Scattering by Droplets of the Mie Size Range, Drexel University Ph.D. Dissertation, 1982.

6. Hetherington, W. M. III, N. E. Van Wyck, E. W. Koenig, G. I. Stegeman, and R. M. Fortenberry, "Observation of coherent Raman scattering in thin-film optical waveguides," Optics Letters 9, 88 (1984).

7. Cloud, Stanley D., and David Wruck, "Size and Refractive Index Dependence of Coherent Anti-Stokes Raman Scattering from Micrometer-Size Polystyrene Spheres," Optics News 10, No. 5, 72 (1984).

8. Wyatt Technology Corporation, 820 East Haley Street, P.O. Box 3003, Santa Barbara California, 93130.

9. Omega Optical, Inc., 3 Grove Street, P.O. Box 573, Brattleboro, Vermont 05301

10. Duke Scientific Corporation, 2415 Embarcadero Way, Palo Alto, California 94303.

11. For example, Snow, Judith B., Shi-Xiong Qian, and Richard K. Chang, "Stimulated Raman scattering from individual water and ethanol droplets at morphology-dependent resonances," Optics Letters 10, 37 (1985).

APPENDIX A

Mathematical Outline of the Procedure for Computing CARS from Spherical Dielectric Particles

I. The outgoing CARS power per unit solid angle is computed from the electromagnetic field amplitude, H:

$$\frac{dP}{d\Omega}(\Theta,\Phi) = \frac{c}{8\pi} r^2 [\vec{H}_3 \cdot \vec{H}_3^*], \text{ where}$$

II. H is computed as an expansion of irreducible tensors:

$$\vec{H}_3 = \frac{e^{ik3r}}{r} \sum_{l} (-i)^{l+1} \sum_{m} CM(l,m)(\vec{r} \times \vec{T}_{llm}) + CE(l,m)\vec{T}_{llm}$$

$$\vec{T}_{llm} = \sum_{\mu} C(l1l;m-\mu,\mu)Y_l^{m-\mu}(\theta,\phi)\hat{\xi}_{\mu} \quad ,$$

III. and the coefficients are:

$$CM(l,m) = -\frac{4\pi n_3 k_3^3 \int \vec{P}^{(3)} \cdot \vec{A}_{lm}^{*in}(M)\, d^3r'}{(xh)'(yj) - n_3(yj)'(xh)}$$

$$CE(l,m) = \frac{4\pi n_3 k_3^3 \int P^{(3)} \cdot \vec{A}_{lm}^{*in}(E)\, d^3r'}{n_3\ (xh)'(yj) - (yj)'(xh)} \quad ,$$

with $\vec{A}_{lm}^{in}(M) = j_l(n_3k_3r)\ \vec{T}_{llm}(\theta,\phi)$

$$A_{lm}^{in}(E) = -\frac{i}{n_3k_3} \vec{\nabla} \times \vec{A}_{lm}^{in}(M),$$

and $\vec{P}^{(3)} = \chi\ \vec{E}(f_1)\vec{E}(f_2)\vec{E}(f_3)$.

n is the refractive index, k the wave number. h and j are the spherical Hankel and Bessel functions. x is k_3a, y is n_3x, and a is the particle radius.

APPENDIX B

THE CRAY-1 PROGRAM "SCARS"

```
      PROGRAM SCARS
      COMMON/PROPS/PI,PMB,RA,REFRAC(3),WAVE1(3),WAVE2(3),LMAX
      COMMON/COORDS/R,COST,SINT,COSP,SINP,P
      COMMON/FIELDS/ER(2),ET(2),EP(2)
      COMMON/RAD2/RB(100),DRB(100)
      COMMON/RAD3/RH(100),DRH(100)
      COMMON/RAD4/RB2(100),DRB2(100)
      COMMON/THETA/PIE(100),TAU(100)
      COMMON/COEFS1/AMIE(100,2),BMIE(100,2)
      COMMON/COEFS2/CMIE(100,2),DMIE(100,2)
      COMMON/HAR/Y(100,100)
      COMMON/CGC/C(3,3,100,100)
      COMMON/TEN/TB(3,3,100,100)
      COMPLEX ER,ET,EP
      COMPLEX TB
      COMPLEX RH,DRH
      COMPLEX AMIE,BMIE
      COMPLEX CMIE,DMIE
      COMPLEX Y
      COMPLEX SM1(3),SM2(3),SE(3),SDB(3)
      COMPLEX DM(100),DE(100)
      COMPLEX CLM(100,100),CLE(100,100)
      COMPLEX AM(3,100,100),AE(3,100,100),APM(100,100),APE(100,100)
      COMPLEX DPROD,IMAGI,CIL
      DIMENSION VL(100),VPL(100)
      SIZEP=70.0
      LMAX=95
      LLMAX=LMAX-1
      CALL CLG
      DO 1 I=1,3
      WAVE1(I)=2.0*PI/WAVE1(I)
C         ABOVE CONVERTS INPUT WAVELENGTHS TO WAVENUMBERS
    1 WAVE2(I)=WAVE1(I)*REFRAC(I)
      RA=SIZEP/WAVE1(1)
      CALL MIECO(1)
      CALL MIECO(2)
C   SAVE CARS 'INSIDE' RICATTI BES. FUNCS. AS RB2 & DRB2
      ARG=WAVE2(3)*RA
      CALL RBES(ARG)
      DO 2 L=1,LMAX
      RB2(L)=RB(L)
      DRB2(L)=DRB(L)
      DL=1.0/FLOAT(L+L+1)
      FL=FLOAT(L)
      VL(L)=SQRT(FL*DL)
      VPL(L)=(FL+1.)*DL
      VPL(L)=SQRT(VPL(L))
    2 CONTINUE
C   CREATE CARS 'OUTSIDE' RIC. HANK. FUNCS.
      ARG=WAVE1(3)*RA
      CALL RBES(ARG)
      CALL RHANK(ARG)
 3000 FORMAT(18H BEGIN INTEGRATION)
C
CBEGIN INTEGRATION TO CREATE CLM(L,M) & CLE(L,M)
C
```

```
      DO 10 I1=21,40
 3100 FORMAT(5H I1= ,I5)
      X=0.05*FLOAT(I1)-1.025
      XS=X*X
      DO 10 I2=21,40
 3200 FORMAT(5H I2= ,I5)
      CY=0.05*FLOAT(I2)-1.025
      YS=CY*CY
      DO 10 I3=1,40
      Z=0.05*FLOAT(I3)-1.025
      ZS=Z*Z
      RS=XS+YS+ZS
      IF(RS.GT.0.998) GOTO 10
      IF(RS.LT.1.E-4) GOTO 10
      R=SQRT(RS)
      COST=Z/R
      RO=SQRT(XS+YS)
      SINT=RO/R
      COSP=X/RO
      SINP=CY/RO
      P=ASIN(SINP)
      CALL INFLD(1)
      CALL INFLD(2)
      DPROD=ER(1)*CONJG(ER(2))+ET(1)*CONJG(ET(2))+EP(1)*CONJG(EP(2))
C     GENERATE A(L,M)S
      ARG=WAVE2(3)*R*RA
      CALL RBES(ARG)
      DO 3 LD=1,LMAX
    3 RB(LD)=RB(LD)/ARG
C           ABOVE MADE SPHER. BESS. FUNC. FROM RICATTI B. F.
      RBO=SIN(ARG)/ARG
      CALL YLM
      CALL TLM
C  AE & AM HERE ARE MULTIPOLE VECTORS, NOT COEFFS.
      DO 5 IC=1,3
      AM(IC,1,1)=TB(IC,2,1,1)*RB(1)
      AM(IC,1,2)=TB(IC,2,1,2)*RB(1)
      AE(IC,1,1)=-VL(1)*TB(IC,3,1,1)*RB(2)+VPL(1)*TB(IC,1,1,1)*RBO
    5 AE(IC,1,2)=-VL(1)*TB(IC,3,1,2)*RB(2)+VPL(1)*TB(IC,1,1,2)*RBO
      DO 9 L=2,LLMAX
      MTOP=L+1
      DO 8 M=1,MTOP
      AM(1,L,M)=TB(1,2,L,M)*RB(L)
      AM(2,L,M)=TB(2,2,L,M)*RB(L)
      AM(3,L,M)=TB(3,2,L,M)*RB(L)
      AE(1,L,M)=-VL(L)*TB(1,3,L,M)*RB(L+1)+VPL(L)*TB(1,1,L,M)*RB(L-1)
      AE(2,L,M)=-VL(L)*TB(2,3,L,M)*RB(L+1)+VPL(L)*TB(2,1,L,M)*RB(L-1)
      AE(3,L,M)=-VL(L)*TB(3,3,L,M)*RB(L+1)+VPL(L)*TB(3,1,L,M)*RB(L-1)
    8 CONTINUE
    9 CONTINUE
C BEGIN NEW L LOOP STARTING WITH L=1
      DO 19 L=1,LLMAX
      MTOP=L+1
      DO 18 M=1,MTOP
      AM(1,L,M)=CONJG(AM(1,L,M))
      AM(2,L,M)=CONJG(AM(2,L,M))
      AM(3,L,M)=CONJG(AM(3,L,M))
      AE(1,L,M)=CONJG(AE(1,L,M))
      AE(2,L,M)=CONJG(AE(2,L,M))
      AE(3,L,M)=CONJG(AE(3,L,M))
   18 CONTINUE
      DO 28 M=1,MTOP
      APM(L,M)=(AM(1,L,M)*ER(1)+AM(2,L,M)*ET(1)+AM(3,L,M)*EP(1))*DPROD
      APE(L,M)=(AE(1,L,M)*ER(1)+AE(2,L,M)*ET(1)+AE(3,L,M)*EP(1))*DPROD
   28 CONTINUE
C     CLM & CLE ARE THEINTEGRALS CALLED SIGMA(M) & SIGMA(E) IN NOTES
```

```
      DO 38 M=1,MTOP
      CLM(L,M)=CLM(L,M)+APM(L,M)
      CLE(L,M)=CLE(L,M)+APE(L,M)
   38 CONTINUE
   19 CONTINUE
   10 CONTINUE
C       CLE(L,M)=CONJG(CLE(L,M))
C     CLM(L,M)=CONJG(CLM(L,M))
 1500 FORMAT(E15.7,3X,E15.7)
C
C    BEGIN S SUM FOR EACH OBSERVATION ANGLE
C
      IMAGI=(0.0,1.0)
      SINP=1.0
      COSP=0.0
      P=PI/2.
      WRITE(12,2000)
      DO 30 L=1,LLMAX
      DM(L)=DRH(L)*RB2(L)-REFRAC(3)*DRB2(L)*RH(L)
   30 DE(L)=REFRAC(3)*DRH(L)*RB2(L)-RH(L)*DRB2(L)
      DO 70 IT=1,179
      FIT =FLOAT(IT)
      T=FIT*PI/180.
      SINT=SIN(T)
      COST=COS(T)
      DO 40 IC=1,3
      SDB(IC)=(0.0,0.0)
   40 CONTINUE
      CIL=-IMAGI
      CALL YLM
      CALL TLM
      DO 60 L=1,LLMAX
      DO 55 IC=1,3
      SM1(IC)=(0.0,0.0)
      SM2(IC)=(0.0,0.0)
   55 SE(IC)=(0.0,0.0)
      MTOP=L+1
      DO 50 M=2,MTOP,2
      SM1(1)=SM1(1)+CLM(L,M)*AIMAG(TB(1,3,L,M))
      SM1(2)=SM1(2)+CLM(L,M)*AIMAG(TB(2,3,L,M))
      SM1(3)=SM1(3)+CLM(L,M)*AIMAG(TB(3,3,L,M))
      SM2(1)=SM2(1)+CLM(L,M)*AIMAG(TB(1,1,L,M))
      SM2(2)=SM2(2)+CLM(L,M)*AIMAG(TB(2,1,L,M))
      SM2(3)=SM2(3)+CLM(L,M)*AIMAG(TB(3,1,L,M))
      SE(1)=SE(1)+CLE(L,M)*AIMAG(TB(1,2,L,M))
      SE(2)=SE(2)+CLE(L,M)*AIMAG(TB(2,2,L,M))
      SE(3)=SE(3)+CLE(L,M)*AIMAG(TB(3,2,L,M))
   50 CONTINUE
      CIL=-CIL*IMAGI
      DO 65 IC=1,3
   65 SDB(IC)=SDB(IC)+CIL*((VL(L)*SM1(IC)+VPL(L)*SM2(IC))/DM(L)-IMAGI*
     CSE(IC)/DE(L))
   60 CONTINUE
 1510 FORMAT(6(E15.7,3X))
      DCS=SDB(1)*CONJG(SDB(1))+SDB(2)*CONJG(SDB(2))+SDB(3)*CONJG(SDB(3))
      DCS=ALOG10(DCS)
      WRITE(12,2100)FIT,DCS
   70 CONTINUE
 1000 FORMAT(F7.3,1X,I3)
 1100 FORMAT(32H TYPE SIZEP(F7.3) SPACE LMAX(I3))
 2000 FORMAT(16H(E15.7,3X,E15.7))
 2100 FORMAT(E15.7,3X,E15.7)
      STOP
      END
      SUBROUTINE MIECO(IN)
      COMMON/PROPS/PI,PMR,RA,REFRAC(3),WAVE1(3),WAVE2(3),LMAX
```

```
      COMMON/RAD2/RB(100),DRB(100)
      COMMON/RAD3/RH(100),DRH(100)
      COMMON/RAD4/RB2(100),DRB2(100)
      COMMON/COEFS1/AMIE(100,2),BMIE(100,2)
      COMMON/COEFS2/CMIE(100,2),DMIE(100,2)
      COMPLEX RH,DRH,AMIE,BMIE,CMIE,DMIE
      X=WAVE2(IN)*RA
      CALL RBES(X)
      DO 10 L=1,LMAX
        RB2(L)=RB(L)
        DRB2(L)=DRB(L)
   10 CONTINUE
      X=WAVE1(IN)*RA
      CALL RBES(X)
      CALL RHANK(X)
      XXX=REFRAC(IN)*PMB
      DO 20 L=1,LMAX
        AMIE(L,IN)=1.0/(PMB*RH(L)*DRB2(L)-REFRAC(IN)*DRH(L)*RB2(L))
        DMIE(L,IN)=1.0/(PMB*DRH(L)*RB2(L)-REFRAC(IN)*RH(L)*DRB2(L))
        BMIE(L,IN)=(REFRAC(IN)*RB(L)*DRB2(L)-PMB*DRB(L)*RB2(L))*
     CDMIE(L,IN)
        CMIE(L,IN)=XXX*(RB(L)*DRH(L)-RH(L)*DRB(L))
        DMIE(L,IN)=CMIE(L,IN)*DMIE(L,IN)
        CMIE(L,IN)=-AMIE(L,IN)*CMIE(L,IN)
        AMIE(L,IN)=(REFRAC(IN)*DRB(L)*RB2(L)-PMB*RB(L)*DRB2(L))*
     CAMIE(L,IN)
   20 CONTINUE
      RETURN
      END
      SUBROUTINE RBES(X)
      COMMON/PROPS/PI,PMB,RA,REFRAC(3),WAVE1(3),WAVE2(3),LMAX
      COMMON/RAD2/RB(100),DRB(100)
      S=SIN(X)
      C=COS(X)
      RIC1=S/X-C
      IF(X.LT.0.9)GO TO 25
      LBIG=LMAX+10
      LBM1=LBIG-1
      RB(LBIG)=0.1
      RB(LBM1)=0.2
      DO 10 L=2,LBM1
        LL=LBIG-L
        LLP1=LL+1
        LLP2=LL+2
        REALIE=2*LL+3
        RB(LL)=REALIE*RB(LLP1)/X-RB(LLP2)
   10 CONTINUE
      SCALE=RIC1/RB(1)
      RB(1)=RIC1
      DRB(1)=S-RB(1)/X
      DO 20 L=2,LMAX
        RB(L)=SCALE*RB(L)
        LM1=L-1
        REALIE=L
        DRB(L)=RB(LM1)-REALIE*RB(L)/X
   20 CONTINUE
      RETURN
   25 RB(1)=RIC1
      RB(2)=3.0*RB(1)/X-S
      DRB(1)=S-RB(1)/X
      DRB(2)=RB(1)-2.0*RB(2)/X
      FRONT=X**3/15.0
      Z=0.5*X*X
      DO 40 L=3,LMAX
        REALIE=2*L+1
        FRONT=FRONT*X/REALIE
```

```
          TERM=1.0
          SERIES=1.0
          NUM=2*L+3
          DO 30 I=1,6
            REALIE =NUM*I
            TERM=-TERM*Z/REALIE
            SERIES=SERIES+TERM
            NUM=NUM+2
   30     CONTINUE
          RB(L)=FRONT*SERIES
          LM1=L-1
          REALIE=L
          DRB(L)=RB(LM1)-REALIE*RB(L)/X
   40 CONTINUE
      RETURN
      END
      SUBROUTINE RHANK(X)
      COMMON/RAD3/RH(100),DRH(100)
      COMMON/RAD2/RB(100),DRB(100)
      COMMON/PROPS/PI,PMB,RA,REFRAC(3),WAVE1(3),WAVE2(3),LMAX
      DIMENSION RN(100),DRN(100)
      COMPLEX RH,DRH
      S=SIN(X)
      C=COS(X)
      RN(1)=-C/X-S
      RN(2)=3.0*RN(1)/X+C
      DRN(1)=-C-RN(1)/X
      DRN(2)=RN(1)-2.0*RN(2)/X
      RH(1)=CMPLX(RB(1),RN(1))
      RH(2)=CMPLX(RB(2),RN(2))
      DRH(1)=CMPLX(DRB(1),DRN(1))
      DRH(2)=CMPLX(DRB(2),DRN(2))
      DO 10 L=3,LMAX
        LM1=L-1
        LM2=L-2
        REALIE=2*L-1
        RN(L)=REALIE*RN(LM1)/X-RN(LM2)
        REALIE =L
        DRN(L)=RN(LM1)-REALIE*RN(L)/X
        RH(L)=CMPLX(RB(L),RN(L))
        DRH(L)=CMPLX(DRB(L),DRN(L))
   10 CONTINUE
      RETURN
      END
      SUBROUTINE INFLD(NW)
      COMMON/PROPS/PI,PMB,RA,REFRAC(3),WAVE1(3),WAVE2(3),LMAX
      COMMON/COORDS/R,COST,SINT,COSP,SINP,P
      COMMON/FIELDS/ER(2),ET(2),EP(2)
      COMMON/RAD2/RB(100),DRB(100)
      COMMON/THETA/PIE(100),TAU(100)
      COMMON/COEFS2/CMIE(100,2),DMIE(100,2)
      COMPLEX ER,ET,EP,CMIE,DMIE,C,IMAGI
      IMAGI=(0.0,1.0)
      RSIZE=WAVE2(NW)*R*RA
      CALL RBES(RSIZE)
      CALL LEG
      ER(NW)=(0.0,0.0)
      ET(NW)=(0.0,0.0)
      EP(NW)=(0.0,0.0)
      C=(1.0,0.0)
      DO 10 L=1,LMAX
        A=2*L+1
        B=L*(L+1)
        ER(NW)=ER(NW)+C*A*CMIE(L,NW)*RB(L)*PIE(L)*SINT
        A=A/B
        C=C*IMAGI
```

```
      ET(NW)=ET(NW)+C*A*(DMIE(L,NW)*RB(L)*PIE(L)-IMAGI*CMIE(L,NW)*      -
     CDRB(L)*TAU(L))
      EP(NW)=EP(NW)+C*A*(IMAGI*CMIE(L,NW)*DRB(L)*PIE(L)-DMIE(L,NW)*      -
     CRB(L)*TAU(L))
   10 CONTINUE
      ER(NW)=ER(NW)*COSP/(RSIZE**2)
      ET(NW)=ET(NW)*COSP/RSIZE
      EP(NW)=EP(NW)*SINP/RSIZE
      RETURN
      END
      SUBROUTINE LEG
      COMMON/PROPS/PI,PMB,RA,REFRAC(3),WAVE1(3),WAVE2(3),LMAX
      COMMON/COORDS/R,X,SINT,COSP,SINP,P
      COMMON /THETA/PIE(100),TAU(100)
      PIE(1)=1.0
      PIE(2)=3.0*X
      TAU(1)=X
      TAU(2)=6.0*X*X-3.0
      DO 10 L=3,LMAX
          LM1=L-1
          LM2=L-2
          REAL1=L
          REAL2=LM1
          REAL3=2*L-1
          PIE(L)=(REAL3*X*PIE(LM1)-REAL1*PIE(LM2))/REAL2
          REAL2=L+1
          TAU(L)=REAL1*X*PIE(L)-REAL2*PIE(LM1)
   10 CONTINUE
      RETURN
      END
      SUBROUTINE YLM
      COMMON/HAR/Y(100,100)
      COMMON/COORDS/R,X,S,COSP,SINP,P
      COMMON/PROPS/PI,PMB,RA,REFRAC(3),WAVE1(3),WAVE2(3),LMAX
       COMPLEX Y
      COMPLEX EIP(100)
      DIMENSION YY(100,100)
      DIMENSION PTM(100),SMP(100),CMP(100)
      NMAX=LMAX+1
      MMAX=NMAX+1
      DO 1 I=1,NMAX
      DO 1 J=1,MMAX
    1 YY(I,J)=(0.0,0.0)
      YY(1,2)=1.
      YY(2,2)=X
      YY(2,3)=-S/SQRT(2.)
      YY(3,2)=(3.*X*X-1.)/2.
      YY(3,3)=-SQRT(1.5)*X*S
      YY(3,4)=SQRT(0.375)*S*S
      DO 100 L=3,LMAX
      FL=FLOAT(L)
      RL=FL-1.
      RLL=FL+RL
      N=L+1
      NL=N-1
      IL=NL-1
      YY(N,2)=(RLL*X*YY(NL,2)-RL*YY(IL,2))/FL
      L2=L-2
      DO 200 M=1,L2
      NM=M+2
      NMM=NM-1
      FM=FLOAT(M)
      PM=FL+FM
      PMM=PM-1.
      PM=FL-FM
```

```
      YY(N,NM)=(SQRT(RM*RMM)*YY(IL,NM)-RLL*S*YY(NL,NMM))/SQRT(PM*PMM)
  200 CONTINUE
      L1=L-1
      DO 300 M=L1,L
      NM=M+2
      NMM=NM-1
      PM=FL+FLOAT(M)
      PMM=PM-1.
      YY(N,NM)=-RLL*S*YY(NL,NMM)/SQRT(PM*PMM)
  300 CONTINUE
  100 CONTINUE
      FPI=0.5/SQRT(PI)
      Y(1,2)=YY(1,2)*FPI
      DO 500 L=1,LMAX
      NP=L+2
      RAD=FLOAT(L+L+1)
      FACT=FPI*SQRT(RAD)
      DO 800 NM=2,NP
      PTM(NM)=FLOAT(NM-2)*P
  800 CONTINUE
      DO 700 NM=2,NP
      SMP(NM)=SIN(PTM(NM))
      CMP(NM)=COS(PTM(NM))
  700 CONTINUE
      DO 900 NM=2,NP
      EIP(NM)=CMPLX(CMP(NM),SMP(NM))
  900 CONTINUE
      DO 400 NM=2,NP
      Y(L+1,NM)=YY(L+1,NM)*EIP(NM)*FACT
  400 CONTINUE
  500 CONTINUE
      DO 600 L=1,LMAX
  600 Y(L+1,1)=-CONJG(Y(L+1,3))
      RETURN
      END
      SUBROUTINE TLM
      COMMON/PROPS/PI,PMB,RA,REFRAC(3),WAVE1(3),WAVE2(3),LMAX
      COMMON/CGC/C(3,3,100,100)
      COMMON/HAR/Y(100,100)
      COMMON/TEN/TB(3,3,100,100)
      COMMON/COORDS/R,CT,ST,CP,SP,P
      COMPLEX TB,Y,T(3,3,100,100),AIM,EIP,CEIP,STP,CSTP,CTP,CCTP
      DO 2 NL=1,LMAX
      MTOP=NL+1
      DO 3 NM=1,MTOP
      T(1,1,NL,NM)=C(1,1,NL,NM)*Y(NL,NM+2)
      T(1,2,NL,NM)=C(1,2,NL,NM)*Y(NL+1,NM+2)
      T(1,3,NL,NM)=C(1,3,NL,NM)*Y(NL+2,NM+2)
      T(2,1,NL,NM)=C(2,1,NL,NM)*Y(NL,NM+1)
      T(2,2,NL,NM)=C(2,2,NL,NM)*Y(NL+1,NM+1)
      T(2,3,NL,NM)=C(2,3,NL,NM)*Y(NL+2,NM+1)
      T(3,1,NL,NM)=C(3,1,NL,NM)*Y(NL,NM)
      T(3,2,NL,NM)=C(3,2,NL,NM)*Y(NL+1,NM)
      T(3,3,NL,NM)=C(3,3,NL,NM)*Y(NL+2,NM)
    3 CONTINUE
    2 CONTINUE
      R2=0.7071067
      AIM=(0.0,1.0)
      EIP=CMPLX(CP,SP)*R2
      CEIP=CONJG(EIP)
      STP=ST*EIP
      CSTP=CONJG(STP)
      CTP=CT*EIP
      CCTP=CONJG(CTP)
      DO 5 NL=1,LMAX
      MTOP=NL+1
```

```
      DO 6 NM=1,MTOP
      TB(1,1,NL,NM)=-STP*T(3,1,NL,NM)+CSTP*T(1,1,NL,NM)+CT*T(2,1,NL,NM)
      TB(2,1,NL,NM)=-CTP*T(3,1,NL,NM)+CCTP*T(1,1,NL,NM)-ST*T(2,1,NL,NM)
      TB(3,1,NL,NM)=-AIM*(EIP*T(3,1,NL,NM)+CEIP*T(1,1,NL,NM))
      TB(1,2,NL,NM)=-STP*T(3,2,NL,NM)+CSTP*T(1,2,NL,NM)+CT*T(2,2,NL,NM)
      TB(2,2,NL,NM)=-CTP*T(3,2,NL,NM)+CCTP*T(1,2,NL,NM)-ST*T(2,2,NL,NM)
      TB(3,2,NL,NM)=-AIM*(EIP*T(3,2,NL,NM)+CEIP*T(1,2,NL,NM))
      TB(1,3,NL,NM)=-STP*T(3,3,NL,NM)+CSTP*T(1,3,NL,NM)+CT*T(2,3,NL,NM)
      TB(2,3,NL,NM)=-CTP*T(3,3,NL,NM)+CCTP*T(1,3,NL,NM)-ST*T(2,3,NL,NM)
      TB(3,3,NL,NM)=-AIM*(EIP*T(3,3,NL,NM)+CEIP*T(1,3,NL,NM))
    6 CONTINUE
    5 CONTINUE
      RETURN
      END
      SUBROUTINE CLG
      COMMON/PROPS/PI,PMB,RA,REFRAC(3),WAVE1(3),WAVE2(3),LMAX
      COMMON/CGC/C(3,3,100,100)
      DO 1 NL=1,LMAX
      L=NL
      NP=L+1
      FL=FLOAT(L)
      D1=FL+1.
      D2=D1+FL+1.
      D3=D2+1.
      D4=2.*FL-1.
      DO 1 NM=1,NP
      M=NM-1
      FM=FLOAT(M)
      FLM=FL-FM
      FPM=FL+FM
      FPM1=FPM+1.
      FLM1=FLM+1.
      FPM2=FPM-1.
      FLM2=FLM-1.
      IF(L-M)2,2,3
    3 C(1,1,NL,NM)=SQRT(FLM*FLM2/2./FL/D4)
    2 C(2,1,NL,NM)=SQRT(FPM*FLM/FL/D4)
      C(3,1,NL,NM)=SQRT(FPM*FPM2/2./FL/D4)
      C(1,2,NL,NM)=SQRT(FLM*FPM1/2./FL/D1)
      C(2,2,NL,NM)=FM/SQRT(FL*D1)
      C(3,2,NL,NM)=-SQRT(FPM*FLM1/2./FL/D1)
      C(1,3,NL,NM)=SQRT(FPM1*(FPM1+1.)/D3/D2)
      C(2,3,NL,NM)=-SQRT(FLM1*FPM1/D1/D3)
      C(3,3,NL,NM)=SQRT((FLM1+1.)*FLM1/D3/D2)
    1 CONTINUE
      RETURN
      END
      BLOCK DATA
      COMMON/PROPS/PI,PMB,RA,REFRAC(3),WAVE1(3),WAVE2(3),LMAX
      DATA REFRAC/1.5213,1.5170,1.5255/
      DATA WAVE1/0.445,0.465,0.426/
      DATA PI/3.1415926536/
      DATA PMB/1.0/
      END
/EOF
EOF
a
```

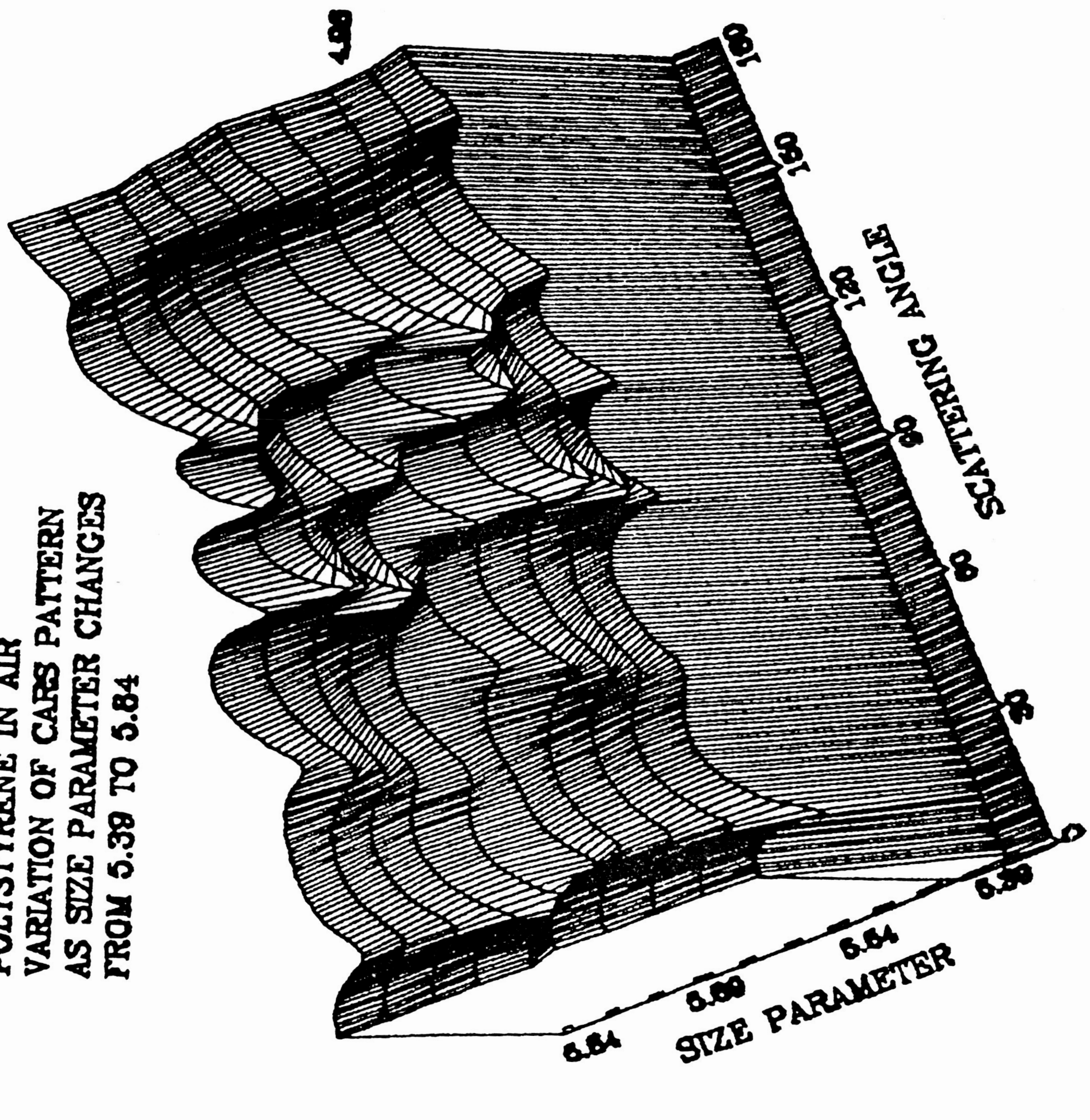

POLYSTYRENE IN AIR
VARIATION OF CARS PATTERN
AS SIZE PARAMETER CHANGES
FROM 5.39 TO 5.84

FIGURE 1

ORIGINAL PAGE IS
OF POOR QUALITY

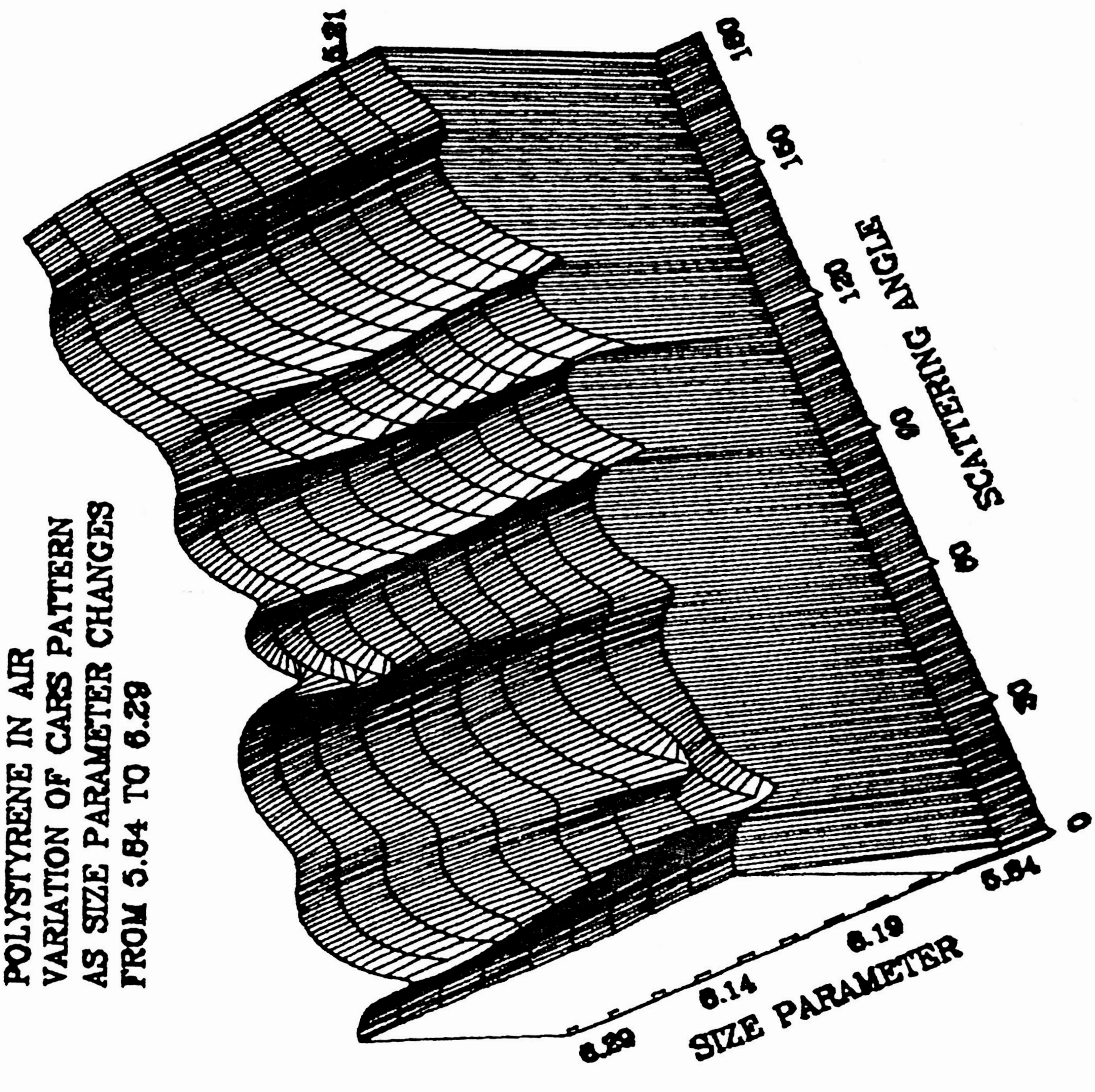

FIGURE 2

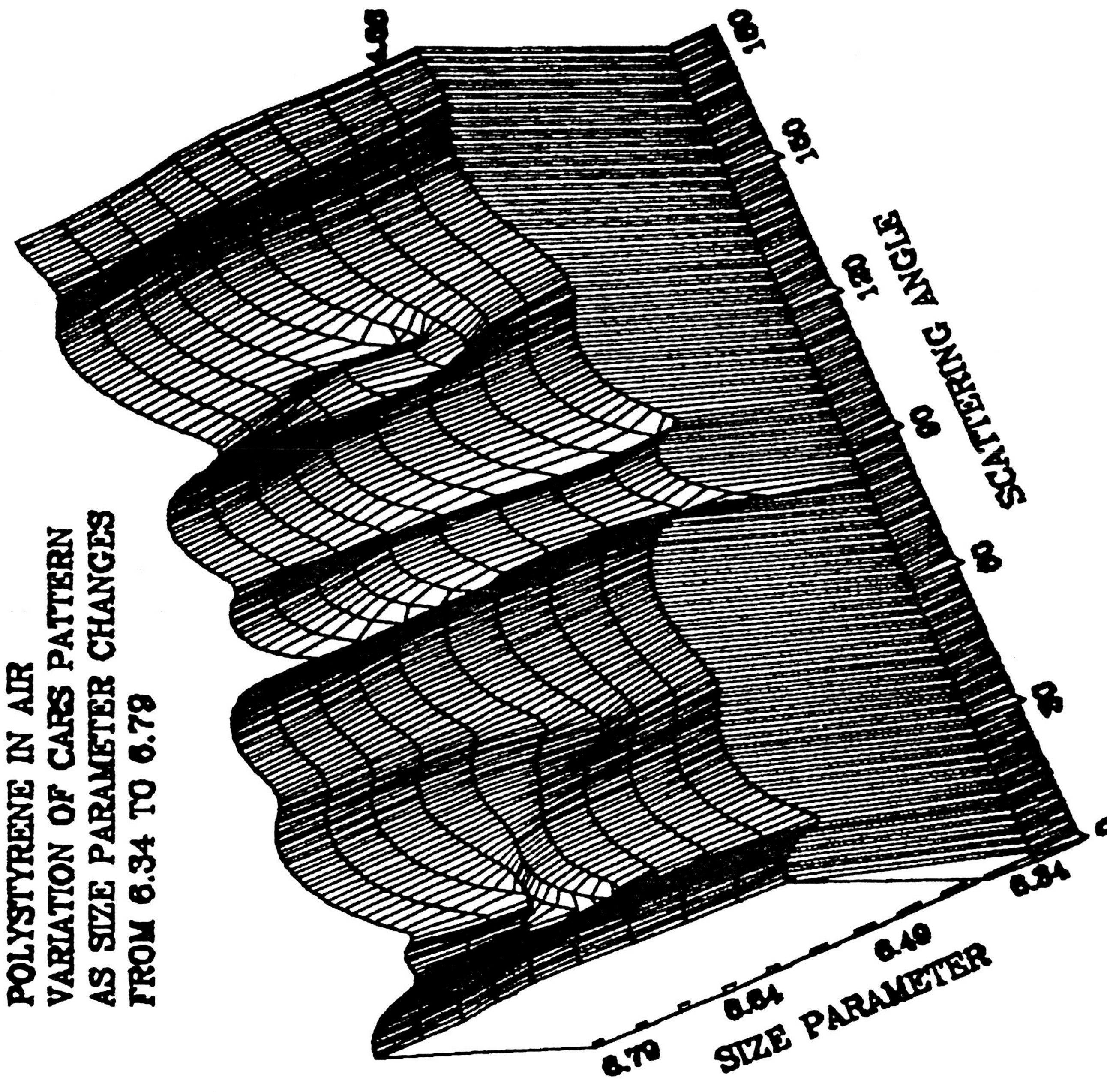
POLYSTYRENE IN AIR
VARIATION OF CARS PATTERN
AS SIZE PARAMETER CHANGES
FROM 6.34 TO 6.79
SCATTERING ANGLE
0
30
60
90
120
150
180
SIZE PARAMETER
6.34
6.49
6.64
6.79

FIGURE 3

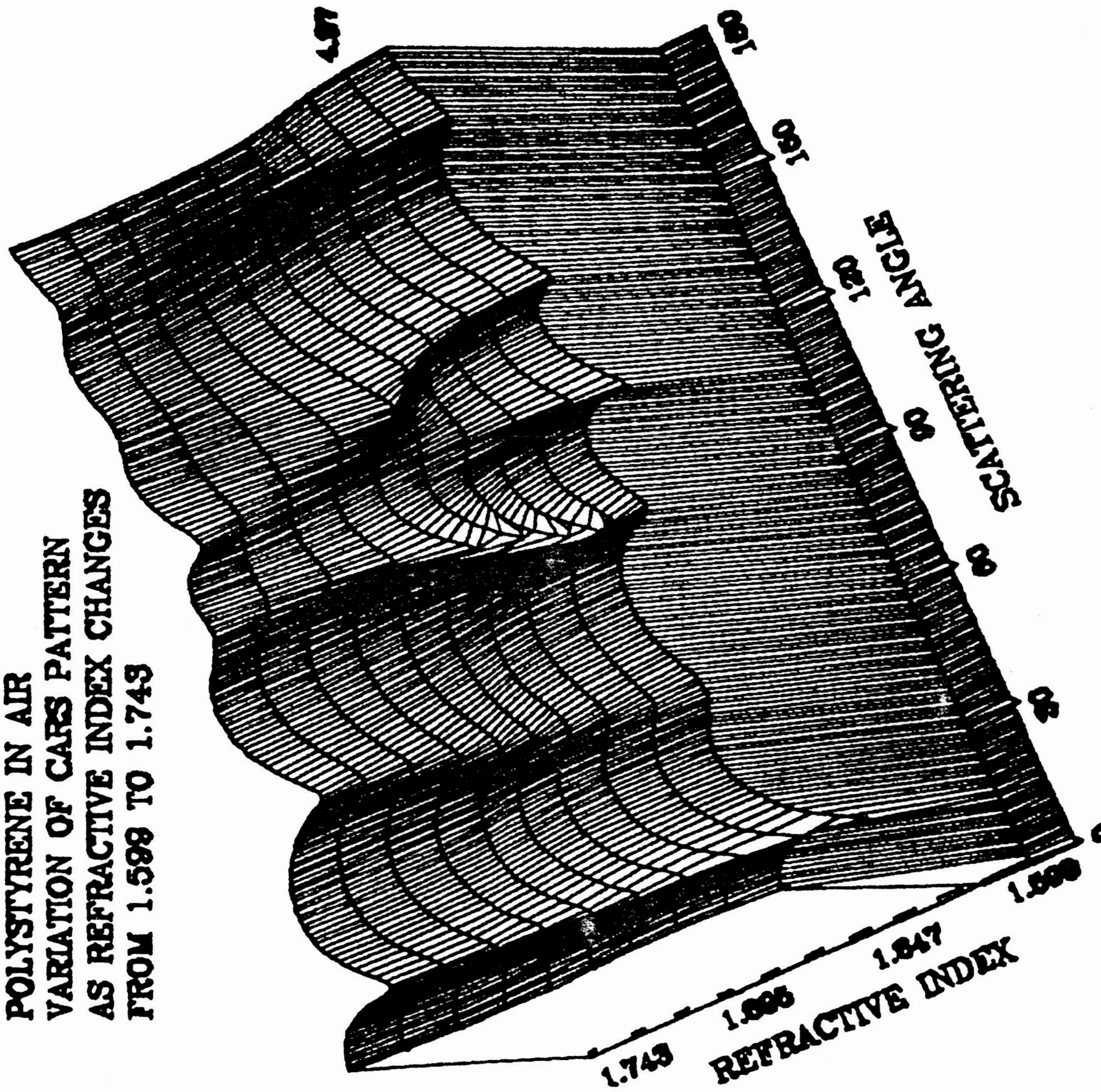
POLYSTYRENE IN AIR
VARIATION OF CARS PATTERN
AS REFRACTIVE INDEX CHANGES
FROM 1.599 TO 1.743
SCATTERING ANGLE
REFRACTIVE INDEX
1.743
1.695
1.647
0
120
180
4.97

FIGURE 4

ORIGINAL PAGE IS
OF POOR QUALITY

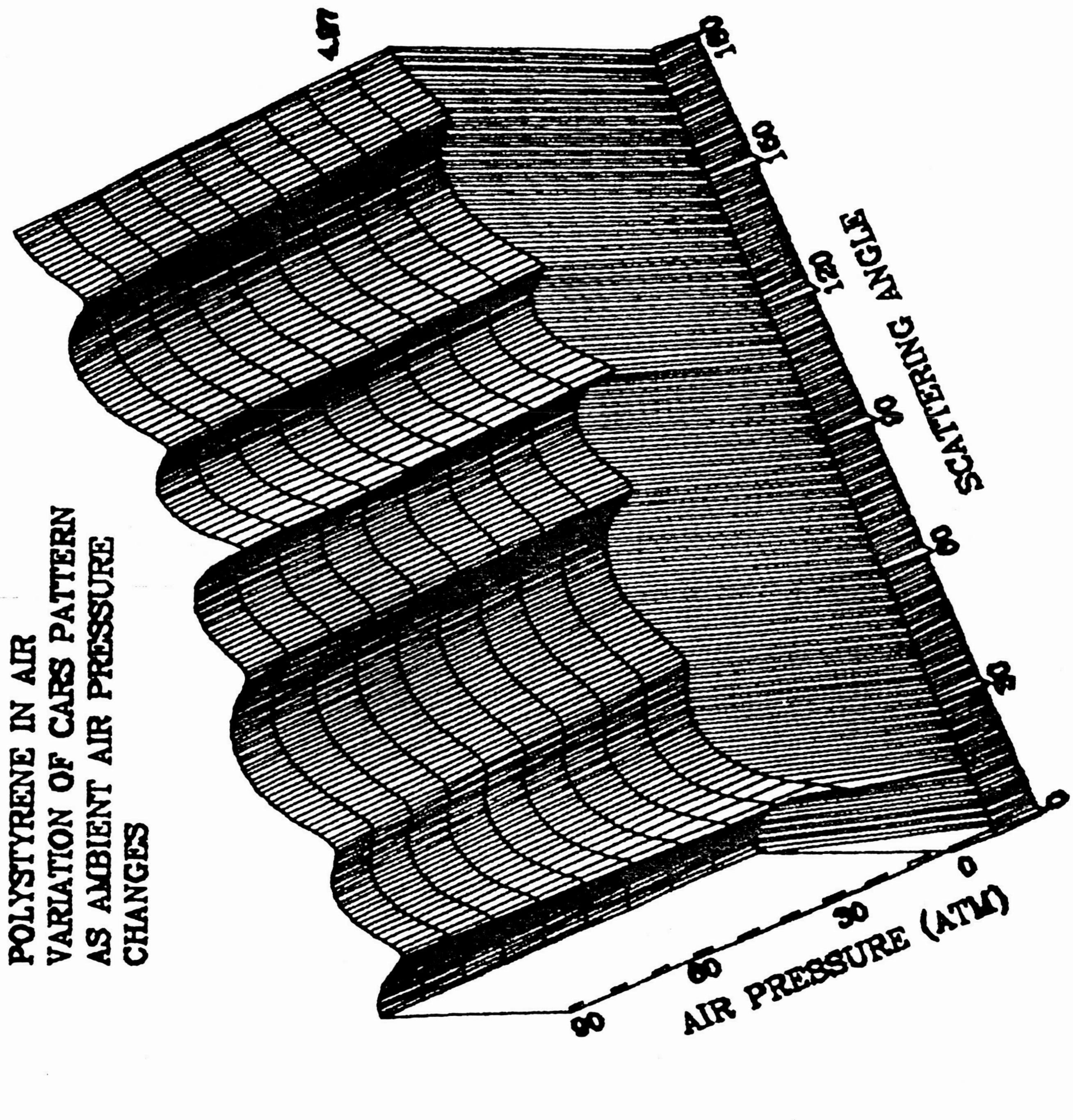

FIGURE 5

ORIGINAL PAGE IS
OF POOR QUALITY

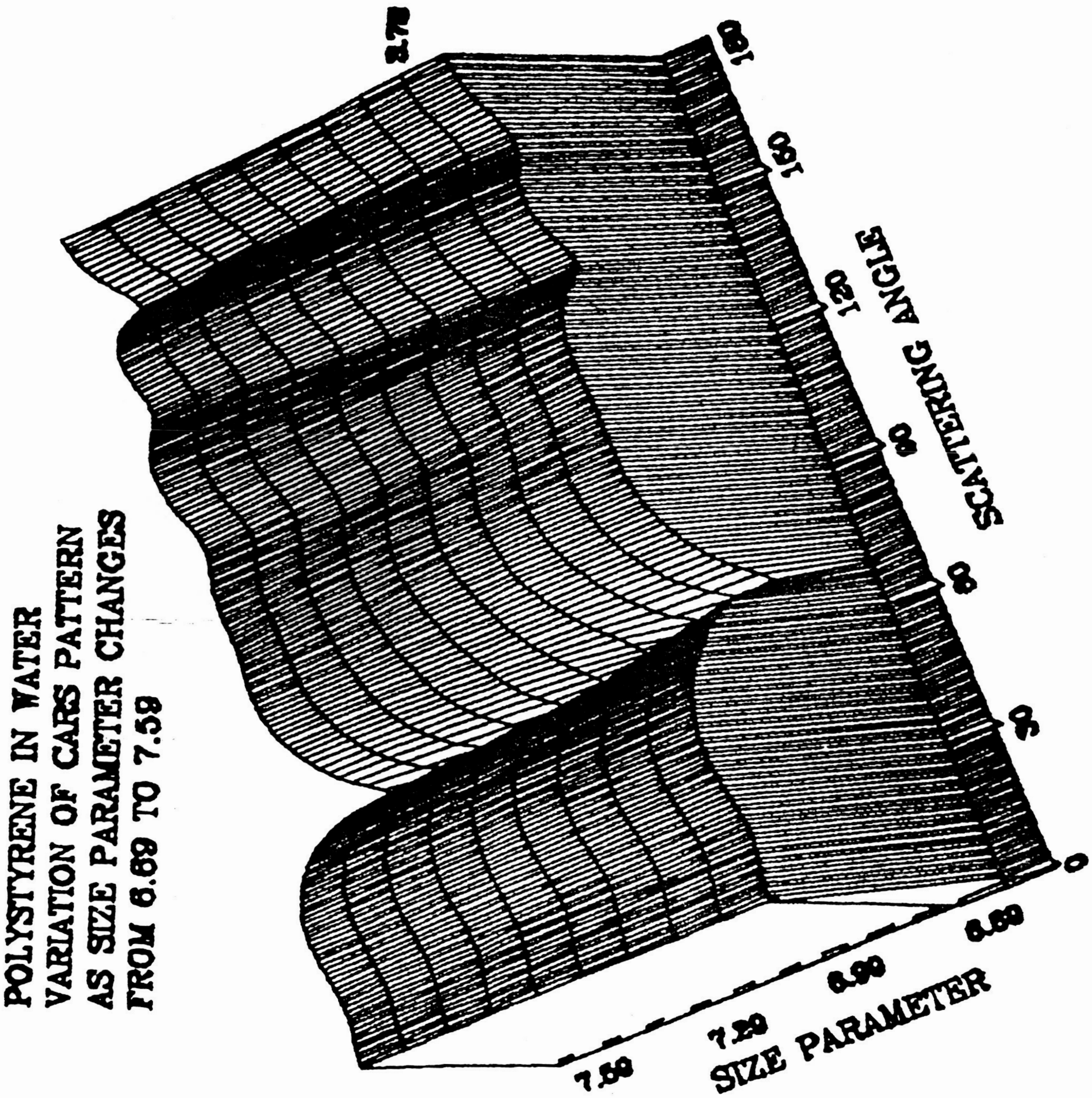

FIGURE 6

ORIGINAL PAGE IS
OF POOR QUALITY

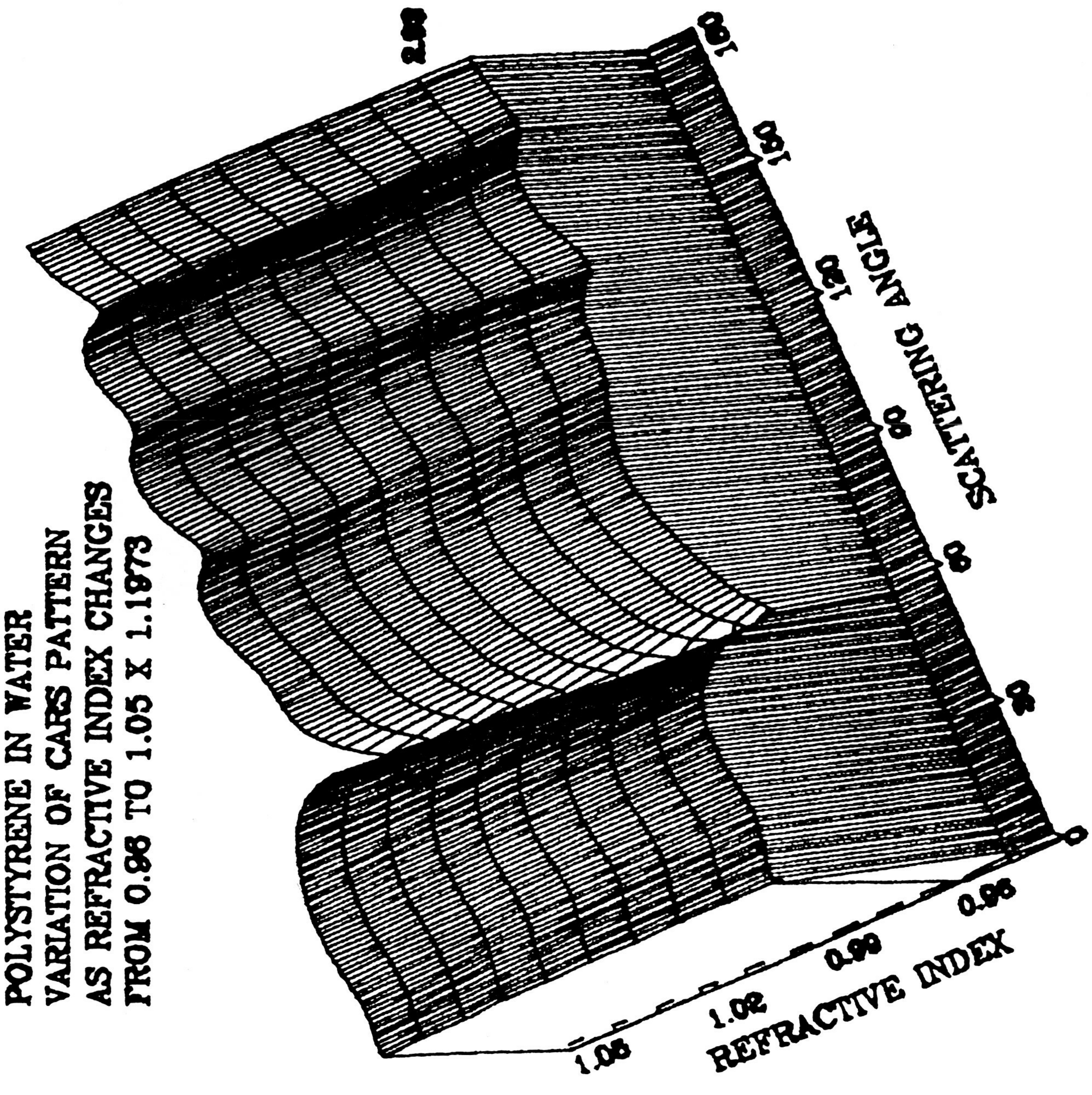

FIGURE 7

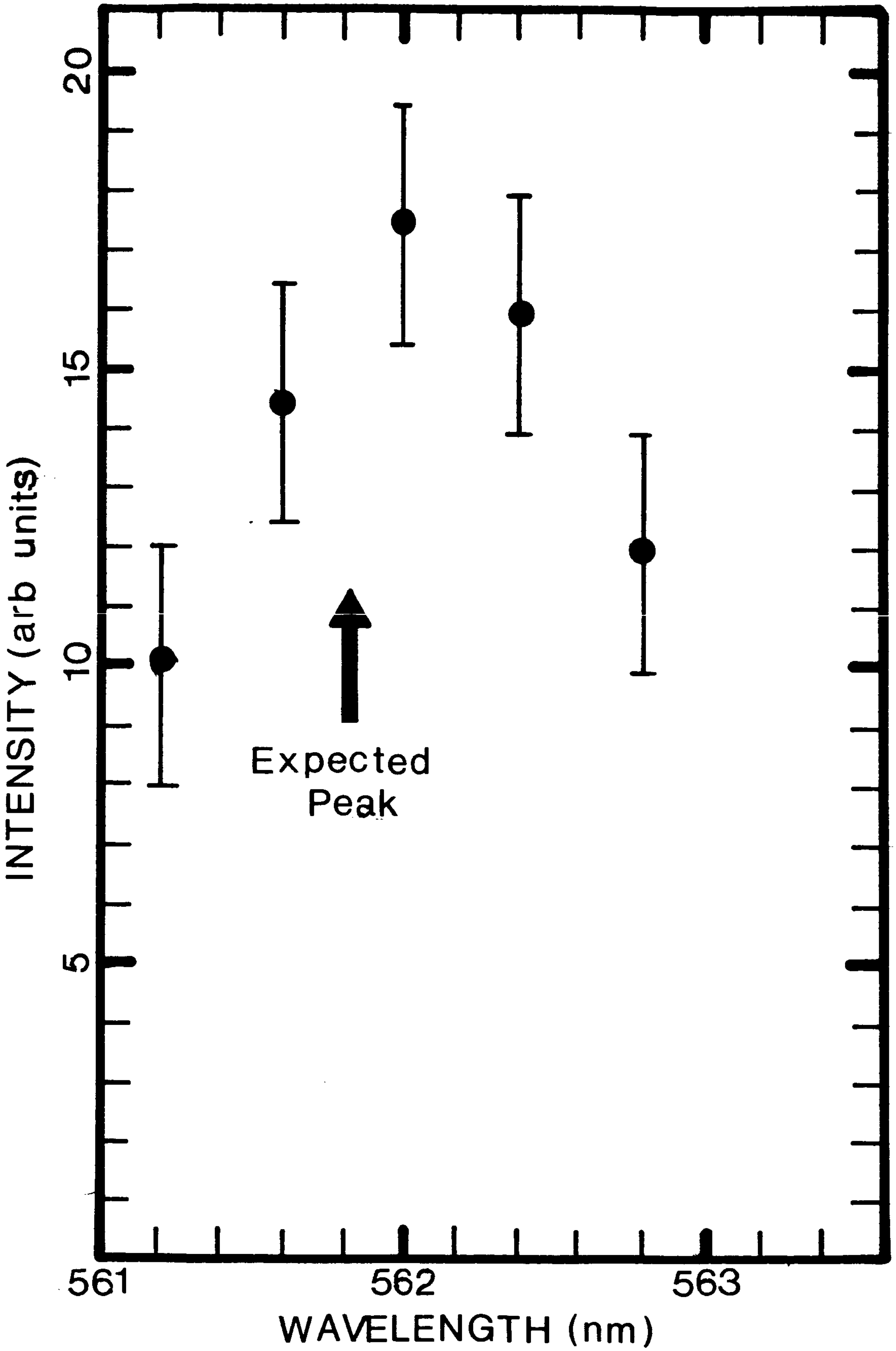

FIGURE 8. Detected Intensity at 505nm as the Dye Laser Wavelength was Varied.